SM22α (Smooth Muscle 22α) Prevents Aortic Aneurysm Formation by Inhibiting Smooth Muscle Cell Phenotypic Switching Through Suppressing Reactive Oxygen Species/NF-κB (Nuclear Factor-κB)

Lintao Zhong, Xiang He, Xiaoyun Si, He Wang, Bing Li, Yinlan Hu, Mengsha Li, Xiaoqiang Chen, Wangjun Liao, Yulin Liao, Jianping Bin

Objective—Vascular smooth muscle cell phenotypic transition plays a critical role in the formation of abdominal aortic aneurysms (AAAs). SM22α (smooth muscle 22α) has a vital role in maintaining the smooth muscle cell phenotype and is downregulated in AAA. However, whether manipulation of the *SM22α* gene influences the pathogenesis of AAA is unclear. Here, we investigated whether SM22α prevents AAA formation and explored the underlying mechanisms.

Approach and Results—In both human and animal AAA tissues, a smooth muscle cell phenotypic switch was confirmed, as manifested by the downregulation of SM22α and α-SMA (α-smooth muscle actin) proteins. The methylation level of the *SM22α* gene promoter was dramatically higher in mouse AAA tissues than in control tissues. SM22α knockdown in $ApoE^{-/-}$ (apolipoprotein E–deficient) mice treated with Ang II (angiotensin II) accelerated the formation of AAAs, as evidenced by a larger maximal aortic diameter and more medial elastin degradation than those found in control mice, whereas SM22α overexpression exerted opposite effects. Similar results were obtained in a calcium chloride-induced mouse AAA model. Mechanistically, SM22α deficiency significantly increased reactive oxygen species production and NF-κB (nuclear factor-κB) activation in AAA tissues, whereas SM22α overexpression produced opposite effects. NF-κB antagonist SN50 or antioxidant N-acetyl-L-cysteine partially abrogated the exacerbating effects of SM22α silencing on AAA formation.

Conclusions—SM22α reduction in AAAs because of the *SM22α* promoter hypermethylation accelerates AAA formation through the reactive oxygen species/NF-κB pathway, and therapeutic approaches to increase SM22α expression are potentially beneficial for preventing AAA formation.

Visual Overview—An online visual overview is available for this article. **(*Arterioscler Thromb Vasc Biol*. 2019;39:e10-e25. DOI: 10.1161/ATVBAHA.118.311917.)**

Key Words: angiotensin II ■ calcium chloride ■ elastin ■ inflammation ■ methylation

Abdominal aortic aneurysm (AAA), defined as a regional dilation of the aortic diameter of >50% compared with the diameter of adjacent aortic tissue, is an important cause of morbidity[1] and is associated with a mortality rate exceeding 80% when ruptured.[2] Pharmacological strategies are accepted as the most fundamental approach for the prevention of AAA. Although pharmacological approaches to prevent the growth and rupture of AAA have been urgently sought, no recognized strategy to halt AAA progression has been developed to date, largely because of an insufficient understanding of the underlying mechanisms of AAA pathogenesis.

The activation of the renin-angiotensin system and abnormal lipid metabolism contribute to AAA formation.[3–5] In fact, a high-fat diet in combination with Ang II (angiotensin II) infusion represents a classic method for constructing an experimental AAA model.[3,4] However, in the clinic, the inhibition of the renin-angiotensin system by angiotensin-converting enzyme inhibitors or angiotensin receptor blockers[6] and the control of plasma LDLs (low-density lipoproteins) by statins are insufficient to prevent AAAs,[7] indicating that novel therapeutic targets may lie downstream of hyperlipidemia and Ang II-activated signaling. The homeostasis of vascular smooth muscle cells (VSMCs) in AAA is disturbed,[5] and VSMC phenotypic switching-mediated vascular pathology contributes to AAA formation.[8,9] Recent studies have documented that SM22α (smooth muscle 22α) is vital in maintaining vascular homeostasis[8] and is downregulated by renin-angiotensin system activation or hyperlipidemia. However, whether the

Received on: May 4, 2018; final version accepted on: October 22, 2018.

From the Department of Cardiology, State Key Laboratory of Organ Failure Research (L.Z., X.H., X.S., H.W., B.L., Y.H., M.L., X.C., Y.L., J.B.) and Department of Oncology (W.L.), Nanfang Hospital, Southern Medical University, Guangzhou, China.

The online-only Data Supplement is available with this article at https://www.ahajournals.org/doi/suppl/10.1161/ATVBAHA.118.311917.

Correspondence to Jianping Bin, MD, PhD, Department of Cardiology, State Key Laboratory of Organ Failure Research, Nanfang Hospital, Southern Medical University, 1838 N Guangzhou Ave, Guangzhou 510515, China. Emails jianpingbin@126.com or jianpingbin@hotmail.com; or Yulin Liao, MD, PhD, Department of Cardiology, State Key Laboratory of Organ Failure Research, Nanfang Hospital, Southern Medical University, 1838 N Guangzhou Ave, Guangzhou 510515, China. Email liao18@msn.com

Nonstandard Abbreviations and Acronyms	
α-SMA	α-smooth muscle actin
AAA	abdominal aortic aneurysm
AAV	adeno-associated virus
Ang II	angiotensin II
ApoE$^{-/-}$	apolipoprotein E–deficient
$CaCl_2$	calcium chloride
CKII	casein kinase II
GFP	green fluorescent protein
IκBα	nuclear factor of κ light polypeptide gene enhancer in B-cells inhibitor-α
IKKβ	inhibitor of NF-κB kinase subunit β
IOD	integral optical density
LDL	low-density lipoprotein
MAC2	galectin 3
MCP-1	monocyte chemotactic protein-1
MMP	matrix metalloproteinase
MYH11	myosin heavy chain 11
NAC	N-acetylcysteine
NF-κB	nuclear factor-κB
PCR	polymerase chain reaction
ROS	reactive oxygen species
siRNA	small-interfering RNA
SIRT1	sirtuin 1
SM22α	smooth muscle 22α
SMC	smooth muscle cell
VSMC	vascular smooth muscle cell

initial disturbance of SM22α has an influence on AAA formation remains unresolved.

Earlier research has revealed significantly downregulated aortic SM22α expression in AAA individuals and animal AAA models.[8–10] Combined with the significance of SM22α in maintaining smooth muscle cell (SMC) structure, we postulate that SM22α inhibits AAA formation by preventing SMC phenotypic switching. To verify this postulation, we examined the aortic expression of SM22α in 2 well-established AAA models, as well as in human AAA tissues. Then, we examined the direct effect of aortic SM22α dysregulation-mediated SMC phenotypic switching on AAA formation. We also investigated the signaling responsible for SM22α disruption in AAA formation and how it regulates AAA formation.

Materials and Methods

The data that support the findings of this study are available from the corresponding author on reasonable request.

Human Aortic Tissue Samples

Human AAA samples were collected from patients undergoing open surgical repair according to protocols approved by Research Ethics Committees of Zhongshan People's Hospital, Sun Yat-sen Hospital, and Guangzhou General Hospital of Guangzhou Military Region. Adjacent nonaneurysmal aortic segments were trimmed from the same patients and used as controls. All aortic tissue samples were used in Western blotting and immunohistochemistry as described previously[11,12] and in bisulfite sequencing polymerase chain reaction (PCR). All procedures comply with the principles of the Declaration of Helsinki (patient clinical information is available in the online-only Data Supplement).

Experimental Animals

Protocols followed the guidelines approved by the Institutional Animal Care and Use Committee at the Southern Medical University. All the animal care and experimental protocols were in accordance with the National Institutes of Health guidelines for the care and use of laboratory animals. Considering the low incidence of experimental AAA in female animals,[13] male mice were used in this study. Male C57BL/6J mice with normal lipid metabolism and male ApoE$^{-/-}$ (apolipoprotein E–deficient) mice on a C57BL/6J background were supplied by the Laboratory Animal Center of Southern Medical University. All mice in the study were fed normal mouse chow. The mice were kept in pathogen-free conditions with a normal chow diet and water under a temperature of 22°C and 60% to 65% humidity with a 12-hour dark/light cycle (lights on at 08:00 AM).

Ang II-Induced AAA Model

Ten- to 12-week-old male wild-type mice and 12- to 16-week-old male ApoE$^{-/-}$ mice were used in these studies. An osmotic minipump (Alzet, Model 2004; DURECT Corporation, Cupertino, CA) was subcutaneously implanted in the dorsum of the neck via a small incision; Ang II (A9525; Sigma, St. Louis, MO) or normal saline was infused via the minipump at a well-established rate[1] of 1 μg/kg per minute for 28 days.[14] A half dose of Ang II infusion (0.5 μg/kg per minute) was also used in this study.

$CaCl_2$-Induced AAA Model

Before undergoing laparotomy, male C57BL/6J mice were anesthetized by intraperitoneally injected pentobarbital (40 mg/kg^{-1}). The abdominal aortic passage below the renal arteries and above the bifurcation of the iliac arteries was isolated from the surrounding retroperitoneal structures. The diameter of this aortic passage was assayed with video microscopy in triplicate. Then, a cotton gauze containing 0.5 mol/L^{-1} $CaCl_2$ was spread onto the external surface of the aortic passage for 15 minutes. NaCl (0.9%) was used for a sham operation in control mice. Then, the aorta was rinsed with 0.9% sterile saline, and the incision was sutured.[15] Mice were euthanized at 3 or 6 weeks after $CaCl_2$ stimulation, and their aortas were harvested for further analysis.

Intervention With N-Acetylcysteine or SN50

As indicated in previous studies, the NF-κB (nuclear factor-κB) blocker SN50 and reactive oxygen species (ROS) antagonist N-acetylcysteine (NAC) were administered to a subset of aortic aneurysm (AA) mice to perform loss-of-function studies. The detailed administration information is listed as follows.

Effect of the NF-κB Antagonist on AA Mice

Ten-week-old male C57BL/6J mice were injected via tail veil with adeno-associated virus (AAV) carrying small-interfering RNA (siRNA) or negative control. At 29 days after infection, mice were randomly assigned to a single intraperitoneal injection of NAC (150 mg/kg per day; n=60)[16] or 1 equivalent infusion of saline (n=60). On the next day, minipump containing Ang II was implanted for 28 days (n=60) or $CaCl_2$ gauze was administrated (n=60) as mentioned above.

Effect of the ROS Antagonist on AA Mice

Ten-week-old male C57BL/6J mice received a single injection of either SN50 (10 μg/kg per day; n=60)[17] or isometric dimethyl sulfoxide (n=60), followed by the same steps mentioned in Effect of the NF-κB Antagonist on AA Mice.

Aneurysm Quantification

Mice were euthanized and cut open ventrally to confirm the existence of an AA. PBS (10 mL) was injected into the left cardiac ventricle

and exited through a cut in the right atrium. Then, the aorta was exposed under a dissecting microscope. The periadventitial tissue was scraped, and the aorta was photographed. The suprarenal aorta was identified as the passage below the last pair of intercostal arteries and above the right renal branch.

The maximum outer width of the abdominal aorta or descending part of the thoracic aorta was measured using Image-Pro Plus software to quantify the AAA size (Media Cybernetics). For quantifying aneurysm incidence, the established human aneurysm definition was adopted, namely, a >50% increase in the outer diameter of the aortas compared with that of aortas from saline-infused mice. Necropsies were performed if mice died during the experimental treatment before being killed. Aortic rupture was defined as the existence of blood clots in the thoracic cavity (thoracic aortic rupture) or in the retroperitoneal cavity (abdominal aortic rupture). Animals that died of aortic rupture were used for the calculation of mortality and rupture rate only and were excluded from tissue degradation analysis. The aneurysm classification (type I–IV) was based on the dilation severity adopted in previous studies, with the following slight amendment[18]: type I, a dilated lumen in the suprarenal aorta, with no or little thrombus formation; type II, a dilated lumen in a prominent bulbous form in the suprarenal aorta, containing a thrombus; type III, dilated lumen with pronounced aneurysms and blood clots from the thoracic aorta through the abdominal aorta; and type IV, subject to ruptured aneurysms.

The intimal and outer width of both the descending thoracic aorta and abdominal aorta was measured as described previously.[4] An evaluation of the AAs was performed by an independent investigator blinded to the experimental treatments. On confirmation of the diameter, area, and aortic classification, a second investigator was invited to match the aneurysm scores to the various treatments of the mice.

Ultrasonography for Aortic Aneurysm

Four weeks after Ang II infusion, surviving mice were anesthetized intraperitoneally with pentobarbital (40 mg/kg^{-1}) and underwent 2-dimensional color-coded ultrasound imaging using a Sequoia ultrasound system with a linear-array ultrasound transducer (15 L8-S; mechanical index, 0.17; frequency, 14 MHz; Siemens Medical Systems).[19]

Histological Analyses

Mice were euthanized, and whole aortas were perfused with saline and fixed with 4% paraformaldehyde at physiological pressure for 5 minutes. The aortas were isolated from the ascending aorta to the entrance of both iliac arteries for macroscopic analysis. Then, the aortas were segmented to obtain suprarenal abdominal aortas (for Ang II-induced AA models) or infrarenal abdominal aortas (for $CaCl_2$-induced AA models). Aortic samples were harvested, fixed for 24 hours, and embedded in paraffin. Histology was examined in cross-sections (5 µm each) that were taken from these aortic samples at intervals of ≈500 µm. At least 10 sections were analyzed per mouse. Paraffin sections were stained with elastin van Gieson staining or used for immunostaining.

Cell Culture and Treatment

Aortic VSMCs (MOVAS-1) were purchased from Guangzhou Geneseed Biotech, Ltd. VSMCs were kept in DMEM with fetal bovine serum (10%), 100 U/mL penicillin, and 100 µg/mL streptomycin. VSMCs were maintained at 37°C in a humidified atmosphere containing 5% CO_2. Cells were used between passages 3 and 6 and were grown to 70% to 80% confluence before being treated with different agents in all experiments. Then, homocysteine solution (25 µg/mL; Sigma) was added to the VSMC medium, and cells were incubated at room temperature for 24 hours,[20] followed by application of the following treatments: (1) the DNA methyltransferase inhibitor 5′-aza-deoxycytidine (5 µmol/L) was incubated at room temperature for 48 hours[21] and (2) PBS was applied as the negative control and incubated at room temperature for 48 hours. At the end of the incubation, VSMCs were obtained and used for SM22α RNA or protein expression assays.

RNA Interference and Cell Transfection

Specific siRNAs against SM22α and nonspecific controls were synthesized by GenePharma (Shanghai, China; sequences of siRNAs are available in the online-only Data Supplement). SM22α siRNA was synthesized by Vigene Bioscience (Jinan, Shandong, China). The overexpression plasmid, pEnter-SM22α (GenBank accession No. NM_011526.5), was synthesized by Vigene Bioscience (Jinan, Shandong, China). VSMCs were seeded into 6-well plates and cultured for 24 hours. Then, 50 nmol/L siRNA or 4 µg pEnter-SM22α was randomly added to 250 µL Opti-Minimum Essential Medium (Gibco BRL, Paisley, United Kingdom) before the addition of 5 µL lipofectamine 3000 (L3000015; Invitrogen). Then, the mixed solution was incubated at room temperature for 0.5 hours and added to the cells. After 6 hours of incubation, the medium was replaced at 37°C with the same volume of DMEM. After 48 hours, the cells were subjected to immunofluorescence analysis, RNA isolation, or protein isolation.

The SM22α AAV was constructed and packaged by Vigene Biosciences (Jinan, China). Specific siRNAs against SM22α and nonspecific controls were separately constructed in one vector, and AAV serotype 9 harboring these sequences was generated by Vigene Biosciences (Jinan, China). Mice were injected one of the above virus (5×10^9 pfu/kg). After 24 hours, the mice were randomly grouped and treated with Ang II or $CaCl_2$ as indicated previously.

Immunohistochemistry Analysis

Mouse samples were deparaffinized, and endogenous peroxidase activity was blocked by 3% (vol/vol) hydrogen peroxide, followed by preincubation with 10% bovine serum to block nonspecific binding sites.[22] Then, slides were incubated at 4°C overnight with primary antibodies (in 1% BSA) and a biotinylated secondary antibody (in 1% BSA) and subsequently incubated with a horseradish peroxidase-labeled streptavidin solution. Then, the slides were stained with diaminobenzidine and counterstained with hematoxylin. The primary antibodies used were mouse SM22α, α-SMA (α-smooth muscle actin), MYH11 (myosin heavy chain 11), MMP (matrix metalloproteinase) 2, MMP9, MAC2 (galectin 3), and rabbit IgG for both Ang II- and $CaCl_2$-induced AA mouse models. Negative control experiments were performed to confirm specificity of antibody binding in Ang II-treated male ApoE$^{-/-}$ mice; information about antibodies is available in the online-only Data Supplement).

Immunofluorescent Staining

Immunofluorescent staining was performed with 5 µm frozen sections from the suprarenal abdominal aortas. Frozen sections were fixed with acetone, followed by blockade with 1% bovine serum in PBS at room temperature for 1 hour and then incubated at 4°C overnight with diluted (AAPR67-100; PanEra) primary antibodies anti-SM22α and anti–H-caldesmon. Secondary antibodies were replaced with antibodies labeled with Alexa Fluor dye with a maximum excitation at 488 nm (green), and for red with Alexa Fluor 568, which were incubated at 37°C for 45 minutes in the dark. Sections were stained simultaneously, using identical reagents and incubation times. The slides were then rinsed with PBS, and images were captured by fluorescence inverted microscope (IX83; Olympus; information about antibodies is available in the online-only Data Supplement).

Elastin Staining and Degradation

The definition and graduation of elastin degradation were described elsewhere.[23] Briefly, suprarenal aortic samples from the different groups of mice were embedded in paraffin, cut, and then measured with Victoria-blue van Gieson staining by applying a commercial kit (GenMed, Shanghai). We used ×40 magnification to evaluate elastin degradation. A previously established standard for the elastin degradation score was adopted as follows[23]: score 1, no elastin degradation,

well-organized elastin lamina; score 2, mild elastin degradation with some interruptions or breaks in the lamina; score 3, moderate elastin degradation with multiple interruptions or breaks in the lamina; and score 4, severe elastin fragmentation or loss or aortic rupture.

Western Blots

Aortic protein expression levels were measured using Western blots as described previously.[24] The separated mouse aortic tissues containing identical amounts of protein were denatured and resolved by 12% sodium dodecyl sulfate-polyacrylamide gel electrophoresis using a 10% running gel. Then, proteins were dissociated using 10% sodium dodecyl sulfate-polyacrylamide gel electrophoresis and probed with primary antibodies for SM22α, MCP-1 (monocyte chemotactic protein-1), MMP2, MMP9, NF-κB P65, β-actin, lamin A/C, RelB, c-Rel, p50, p52, IKKβ (inhibitor of NF-κB kinase subunit-β), p-IKKβ, IκBα (nuclear factor of κ light polypeptide gene enhancer in B-cells inhibitor-α), p-IκBα, or caspase-3 at 4°C overnight. All primary antibody reagents were diluted by AAPR67-100 (PanEra). Next, the membranes were washed and incubated with a horseradish peroxidase-conjugated anti-rabbit secondary antibody at a 1:5000 dilution (DAKO) for 2 hours. β-actin was used as a loading control. Bands were detected using enhanced chemiluminescence (Advance, No. RPN2235; GE Healthcare Life Sciences). The protein intensity was determined, quantified, and normalized to that of β-actin by using a ChemiDoc imaging system (Bio-Rad Laboratories), and ImageJ Analysis software (National Institutes of Health, Bethesda, MD) was used for protein expression analysis. All experiments were replicated 3×; information about antibodies is available in the online-only Data Supplement).

MMP2 and MMP9 Quantification

Quantification of MMP2 and MMP9 was determined by using IPP software, based on the integral optical density (IOD) value, the sum of the chroma, and acreage of positive color (claybank). The mean IOD was calculated as the IOD value divided by the acreage of the samples. Each specimen had 3 lower power sections and 9 higher power sections. The mean IOD was the mean value of the IOD value in the 9 higher power sections.

Quantitative Real-Time PCR

Total RNA of ex vivo VSMCs or of aortic tissues from different mouse groups was extracted by homogenization using TRIzol reagent (Invitrogen) according to the manufacturer's protocol and then converted to cDNA following standard methods. cDNA was synthesized by reverse transcriptase (Takara Biotechnology, Dalian, China) using the primer sequences for the examined molecules. Real-time PCR was performed with a SYBR Green RT-PCR Kit (Takara Biotechnology) using Light Cycler 480 II equipment (Roche Diagnostics, Basel, Switzerland). The relative expression of mRNA was determined using the 2-ΔΔCt method by normalizing the expression against that of β-actin. Primers were synthesized by Saicheng Biotech (Guangzhou, China; primers for quantitative real-time PCR are available in the online-only Data Supplement).

Immunoprecipitation

Coimmunoprecipitation was conducted using an antibody against phosphorylated-Ser, and the precipitation was performed via coincubation with an antibody against $p47^{phox}$. Briefly, total protein extracts from aortic wall were pretreated 50 mmol/L Tris-HCl (pH 8), 150 mmol/L NaCl, 1% Nonidet P-40, and protease (1 mmol/L phenylmethylsulfonyl fluoride, 40 μg/mL^{-1} aprotinin, and 40 μg/mL^{-1} leupeptin) and phosphatase (1 mmol/L sodium orthovanadate and 1 mmol/L NaF) inhibitors, followed by incubation with 5 μg (per 200 μg protein) of a rabbit monoclonal antibody against phosphorylated-ser primer antibody reagents were diluted by primary antibody dilution buffer (AAPR67-100; PanEra). Bound proteins were precipitated with anti-rabbit IgG beads (cat 8800; eBioscience, San Diego, CA) for 1 hour with rocking at 4°C, followed by incubation with protein A-agarose overnight at 4°C; then, the proteins were resolved by sodium dodecyl sulfate-polyacrylamide gel electrophoresis, and Western blots were performed as described above (information about antibodies is available in the online-only Data Supplement).

ROS Analysis

For the detection of vascular ROS activity, suprarenal abdominal aortas were harvested and embedded vertically in tissue optimal cutting temperature freezing medium (Tissue-Tek; Miles, Elkhart, IL), snap-frozen, cross-sectioned (7 mm), and then incubated with dihydroethidium (5 mol/L^{-1}; Sigma) for 30 minutes at 37°C. Sections were examined by using a fluorescence inverted microscope (Leica Imaging Systems, Cambridge, United Kingdom) to reveal the existence of ROS as red fluorescence (585 nm).[23]

Bisulfite Sequencing PCR

The methylation status of the promoter regions of *SM22α* in human and mouse AA samples was detected by bisulfite sequencing PCR. Bisulfite sequencing PCR-specific primer pairs for the *SM22α* gene were generated with MethPrimer (http://www.urogene.org/methprimer/; bisulfite sequencing PCR-specific primer is available in the online-only Data Supplement).The human and mouse *SM22α* gene CpG island regions contained 15 and 10 CpG dinucleotides, respectively. The human *SM22α* gene contained promoter regions spanning from −290 to −32 bp relative to the transcription start site of human *SM22α* transcript variant 1. The mouse *SM22α* gene contained promoter regions spanning from −222 to −3 bp relative to the transcription start site of mouse *SM22α* transcript variant 1. DNA was treated with bisulfite and amplified with PCR under the following conditions (as in previous studies): denaturation at 95°C for 5 min; 30 cycles of 95°C for 30 s, 55°C for 30 s, and 72°C for 30 s, with extension for 10 minutes at 72°C. The amplified products were then gel purified and cloned into a pMD 19-T vector (Invitrogen). Ten clones from each sample were randomly selected for plasmid DNA extraction with a Qiagen Plasmid Mini Kit (Qiagen) and DNA sequencing.

Statistical Analysis

Values are presented as the mean±SD. The data were analyzed using SPSS, version 20.0 (SPSS, Inc, Chicago, IL). Normal distribution test was performed for all continuous variables. After confirmation of variance equality among different groups, statistical differences between 2 independent groups were analyzed using unpaired Student *t* test, whereas statistical difference among ≥3 groups was analyzed using 1- or 2-way ANOVA followed by post hoc test of Dunnett. If a normal distribution could not be determined, nonparametric tests were applied Mann-Whitney *U* test for 2 independent groups. Fisher exact test was applied for the analysis of aneurysm incidence. The correlation between gene promoter methylation status and the expression of the VSMC *SM22α* gene was explored by Spearman correlation. $P < 0.05$ was considered statistically significant.

Results

SM22α Is Downregulated in Human and Mouse AAA Tissues

Human intimal and medial AAA sections and the corresponding adjacent normal aortic tissues were obtained from patients undergoing AAA resection surgery. Western blotting results showed that the protein expression of SM22α was remarkably lower in AAA tissues than in corresponding adjacent normal aortic tissues ($P<0.01$) and was accompanied by significantly elevated MMP2 ($P<0.05$) and MMP9 ($P<0.01$), which are 2 extracellular matrix proteolytic enzymes that are crucially implicated in AAA formation (Figure 1A). Immunohistochemistry staining confirmed that the levels of

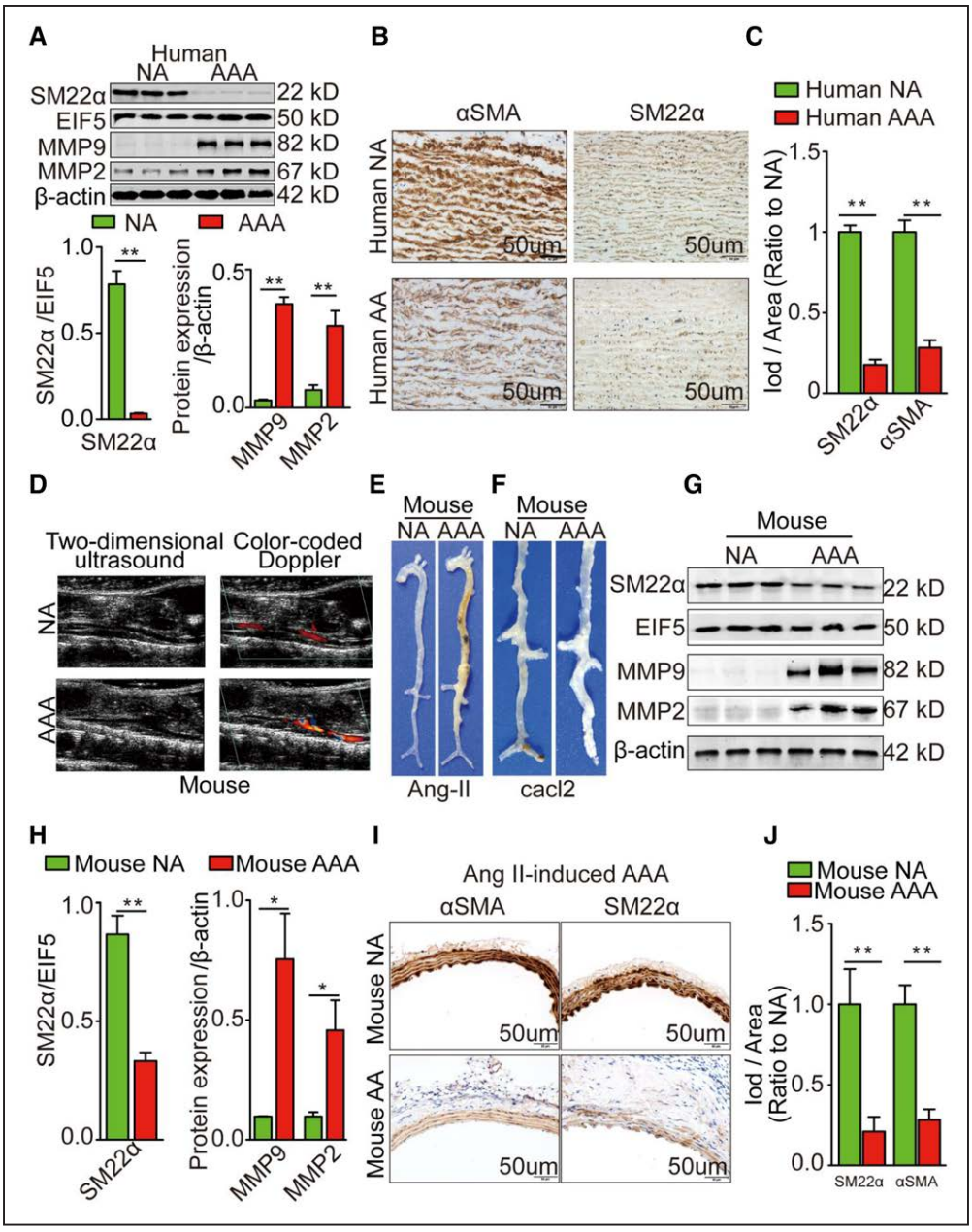

Figure 1. SM22α (smooth muscle 22α) is decreased in human aortic aneurysm samples and in Ang II (angiotensin II)-induced mouse aortas. **A**, Western blots (WB) and densitometric analysis of the protein levels of SM22α, MMP (matrix metalloproteinase) 9, and MMP2 in human abdominal aortic aneurysm (AAA) samples and adjacent nonaneurysmal aortic sections (male; n=3). **B** and **C**, Representative staining with α-SMA (α-smooth muscle actin) and SM22α in human AAA samples and adjacent control aortas (scale bars=50 μm). The photographs were taken at the location where the most severe aortic dilation occurred. **D**, Two-dimensional ultrasound and color-coded Doppler imaging of aortic aneurysm development and complications at 14 d after Ang II infusion in male ApoE$^{-/-}$ (apolipoprotein E–deficient) mice. **E** and **F**, Representative photographs showing the macroscopic features of aortic aneurysms in at 28 d after Ang II infusion in male ApoE$^{-/-}$ mice (1 μg/kg per min) or at 3 wk after $CaCl_2$ treatment in male C57BL/6J mice. **G** and **H**, WB and densitometric analysis of the protein levels of SM22α, MMP9, and MMP2 in AAs from Ang II-induced male ApoE$^{-/-}$ mice and control male ApoE$^{-/-}$ mice (n=3). **I** and **J**, Representative immunohistochemical staining with α-SMA and SM22α in suprarenal AAs from male ApoE$^{-/-}$ mice treated with Ang II and control male ApoE$^{-/-}$ mice. Data are presented as the mean±SD. *P<0.05, **P<0.01. NA indicates nonaneurysmal aorta.

SM22α, α-SMA, and MYH11, which are markers of SMCs, were substantially decreased in human aortic medial SMCs compared with those in adjacent nonaneurysmal SMCs (P<0.01; Figure 1B and 1C; Figure IB in the online-only Data Supplement).

We further investigated the expression of SM22α in the AAA mouse model. As shown by 2-dimensional ultrasonography and color-coded Doppler imaging, a dilated abdominal aorta was seen at 14 days after Ang II infusion in ApoE$^{-/-}$ mice (Figure 1D). Macroscopy showed formed aneurysm at 28 days after Ang II infusion in ApoE$^{-/-}$ mice (Figure 1E) or at 3 weeks after $CaCl_2$ treatment in C57BL/6J mice (Figure 1F), but not in their control counterparts, suggesting successful AAA modeling. Findings about the tendencies of SM22α (P<0.01), α-SMA, MYH11, and MMP2/9 (P<0.01; Figure 1G through 1J; Figure IC and ID in the online-only Data Supplement) were

concordant between human AAA and mouse AAA. These findings were consistent with the findings during the process of SMC phenotypic switching to some extent.

Hypermethylation of the *SM22α* DNA Promoter Occurs in Human and Mouse AAA Tissues

We explored whether decreased SM22α expression during AAA formation is relevant to the enhanced methylation level of the *SM22α* gene promoter. A bisulfite sequencing PCR technique was adopted to detect methylated CpG sites (CpG islands) in both human and mouse *SM22α* promoters (Figure 2A and 2B). Five samples from human AAAs and adjacent normal specimens (Figure 2C) and 5 samples from Ang II-induced ApoE$^{-/-}$ mouse AAAs and adjacent normal aortic tissues (Figure 2D) were assessed. Each mouse sample was a mixture of aortic tissues from 3 individual specimens. Thus, an adequate amount of aortic tissue was obtained for measurements. The percentage of methylated CpG sites in the *SM22α* promoter was substantially higher in human AAA samples and in mouse Ang II-induced AAA samples than in their respective control samples (Figure 2B and 2D; $P<0.01$). Similar results were found 28 days later in $CaCl_2$-induced AAA mice compared with those in sham-control mice (Figure 2E; $P<0.05$). Because SMC phenotypic switching already occurs in the early phase of AAA pathogenesis, we explored whether the *SM22α* gene promoter underwent significant DNA methylation alterations in the early days. Accordingly, *SM22α* promoter methylation levels in aortic VSMCs were detected on the first, fourth, and seventh day after Ang II treatment. Compared with the control group, the Ang II group showed a mild but nonsignificant increase in methylated nucleotides in the mouse aortic *SM22α* promoter on the first day (Figure 2F). This upregulation became significant 4 ($P<0.05$) and 7 ($P<0.05$) days after Ang II administration (Figure 2F and 2H). We further detected the aortic SM22α production rate during this period and found significant reductions in SM22α mRNA levels (Figure IIB in the online-only Data Supplement) and protein expression levels (Figure IIC and IID in the online-only Data Supplement) on the fourth ($P<0.01$) and seventh day ($P<0.01$) compared with those on the first day. Importantly, we accordingly identified a negative association between the SM22α expression level and *SM22α* promoter methylation status (Figure IIA in the online-only Data Supplement). Furthermore, an appropriate dose of 5′-aza-deoxycytidine—a DNA demethylating agent—was administered to ex vivo VSMCs for 24 hours. Consequently, the *SM22α* gene exhibited substantially increased SM22α transcription ($P<0.01$) and protein expression ($P<0.01$; Figure IIE through IIG in the online-only Data Supplement) in VSMCs. We further evaluated dnmt levels in human AAA and Ang II- or $CaCl_2$-induced mouse AAA and found that dnmt1 and dnmt3b but not dnmt3a were substantially upregulated in human and mouse AAA specimens (Figure IIIA through IIIC in the online-only Data Supplement). The significant upregulation of dnmt1 and dnmt3b in mouse aortic tissue started at the fourth day after Ang II stimulation (Figure IIID through IIIF in the online-only Data Supplement). In conclusion, hypermethylation of the *SM22α* gene is associated with upregulation of dnmt1 and dnmt3b and may contribute to the epigenetic silencing of SM22α expression in AAA.

Targeting SM22α Influences the Development of AAA

To further identify a potential causative link between disturbed SM22α expression and AAA development, we selected an AAV carrying SM22α siRNA or SM22α overexpression plasmid to perform gain- or loss-of-function studies in Ang II-perfused ApoE$^{-/-}$ mice AAV-GFP (green fluorescent protein), AAV-SM22α, Scr-RNA, and sh-SM22α groups. First, 4 siRNA sequences and pcDNA3.1-SM22α were separately and successfully integrated into transfected cultured VSMCs. The detection of SM22α mRNA levels in ex vivo VSMCs reflected that siRNA 1 and pcDNA3.1 were the most potent in inhibiting and promoting SM22α expression, respectively (Figure IVA and IVB in the online-only Data Supplement). Serial aortic SM22α protein expression levels were assessed on the 15th, 30th, 40th, 50th, and 60th days (Figure IVC in the online-only Data Supplement). Beginning at the 30th day, as anticipated, both knockdown and overexpression interventions yielded significant and continuous inhibition and promotion of SM22α expression, respectively, compared with that yielded by no intervention (Figure 3A and 3B). Moreover, compared with the saline control group, both the sh-SM22α group and AAV-SM22α group had a significantly enhanced aortic GFP signal, indicating a high efficiency of viral transfection (Figure VA and VB in the online-only Data Supplement). Then, on the 30th day, a proportion of the ApoE$^{-/-}$ mice was randomly selected to start receiving an Ang II infusion for 28 days (Figure IVD in the online-only Data Supplement). Considering that SM22α has been reported to promote transition of adventitial fibroblasts to a myofibroblast phenotype,[25] we further evaluated whether adventitial fibroblasts can affect the role of SM22α on AAA. Results of coimmunofluorescence staining with SM22α and H-caldesmon revealed that the H-caldesmon–stained areas were overlapped with the SM22α-stained areas, indicating that SMCs but not aortic adventitial fibroblasts were affected by AAV intervention (Figure XVA in the online-only Data Supplement). Furthermore, PCR and Western blotting detection of aortic adventitial SM22α demonstrated that no significant different SM22α expressions were noted between AAV-SM22α and AAV-GFP groups (Figure XVB and XVC in the online-only Data Supplement).

After 14 days of Ang II infusion, bulges were detected by 2-dimensional ultrasonography and color-coded Doppler imaging in the mice abdominal aorta of sh-SM22α group (Figure 3F). After 28 days of Ang II infusion, aortic SM22α protein expression levels in both the descending thoracic aorta (Figure VIC in the online-only Data Supplement) and abdominal aorta (Figure 4C) were detected by immunohistochemical staining. There was a substantial enhancement of AAA formation in the sh-SM22α group compared with that in the sham Scr-RNA group (30 of 32 mice, 93.7%; 30 AAAs; 3, 2, 13, and 12 specimens with an AA classification of I, II, III, and IV, respectively, in the sh-SM22α group; 22 of 32 mice, 68.8%; 22 AAAs; 4, 7, 1, and 10 with an

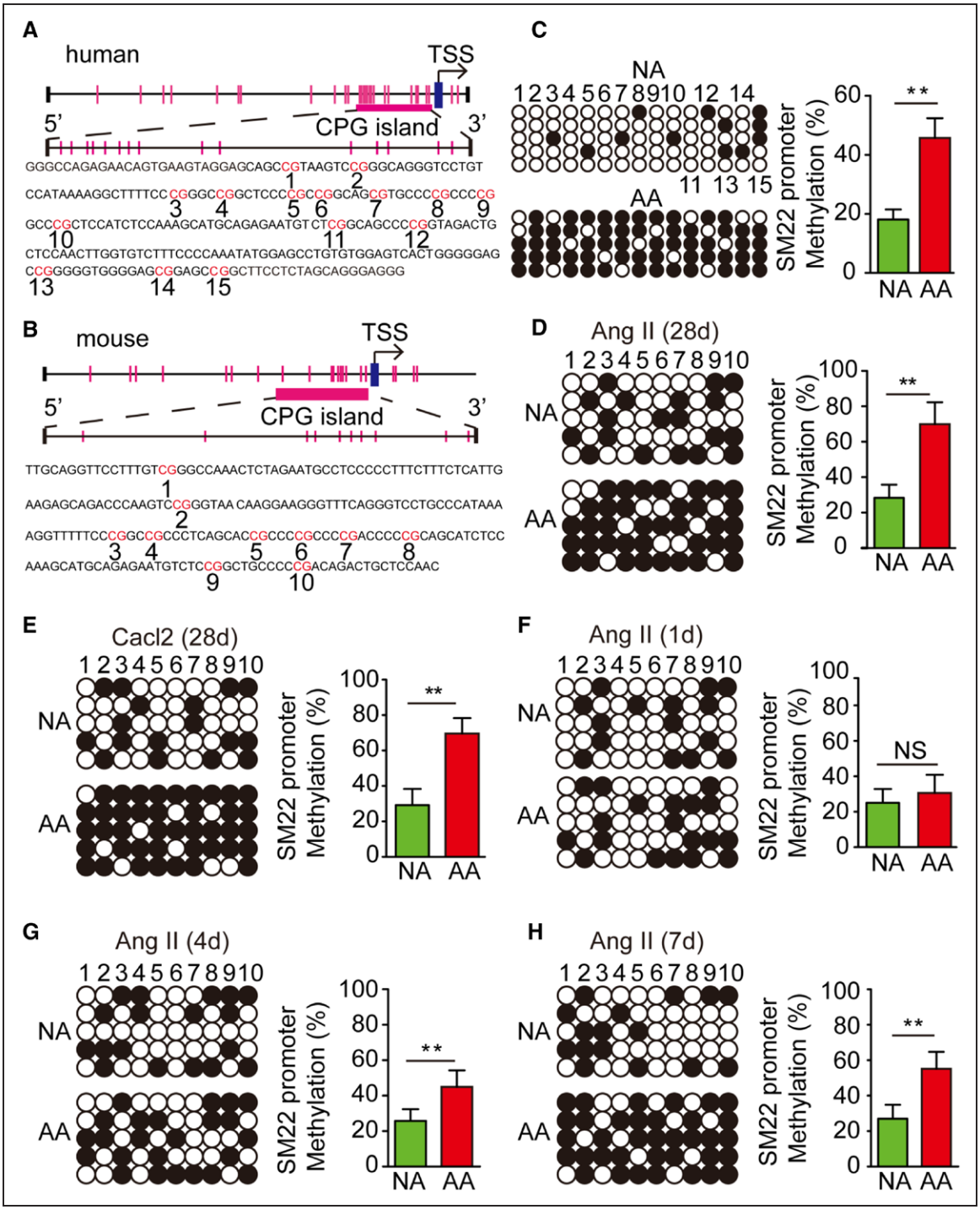

Figure 2. Methylation status of the *SM22α* (smooth muscle 22α) promoter in the human aneurysmal aorta and in Ang II (angiotensin II)- and $CaCl_2$-induced aortic aneurysms. **A** and **B**, Schematic representing the distribution of CpG sites in *SM22α* genes from a human aortic section (male; **A**) and an Ang II-induced male $ApoE^{-/-}$ (apolipoprotein E–deficient) mouse aorta (**B**) with the selected CpG island of a 269-bp fragment (–290 to –32 bp) and a 220-bp fragment (–222 to –3 bp) relative to the transcription start site. The transcription start site is indicated by a curved arrow. Each vertical bar represents a single CpG site. **C**–**E**, Bisulfite sequencing polymerase chain reaction (BSP) results of selected CpG loci within the *SM22α* gene promoter region from human aortas (male; n=5; **C**), Ang II-induced male $ApoE^{-/-}$ mice (n=10; **D**), and $CaCl_2$-treated male C57BL/6J mice (at 3 wk after treatment; n=10; **E**). Quantitative analyses of the methylation status indicated by the numbers of selected CpG are presented. Five colonies of polymerase chain reaction products from each bisulfite-treated DNA sample were sequenced, and each is presented as an individual row. One circle indicates one CpG site, and closed or open circles represent methylated or unmethylated cytosines, respectively. **F**–**H**, BSP sequencing results of selected CpG loci within the *SM22α* gene promoter region from male C57BL/6J mouse aortas 1 (**F**), 4 (**G**), and 7 d (**H**) after Ang II stimulation (n=10). Quantitative analysis of the methylation status indicated by the numbers of selected CpG is presented. Tissues from 3 mice were pooled as one sample. Data are presented the mean±SD. ***P*<0.01. AA indicates aortic aneurysm; and NS, not significant.

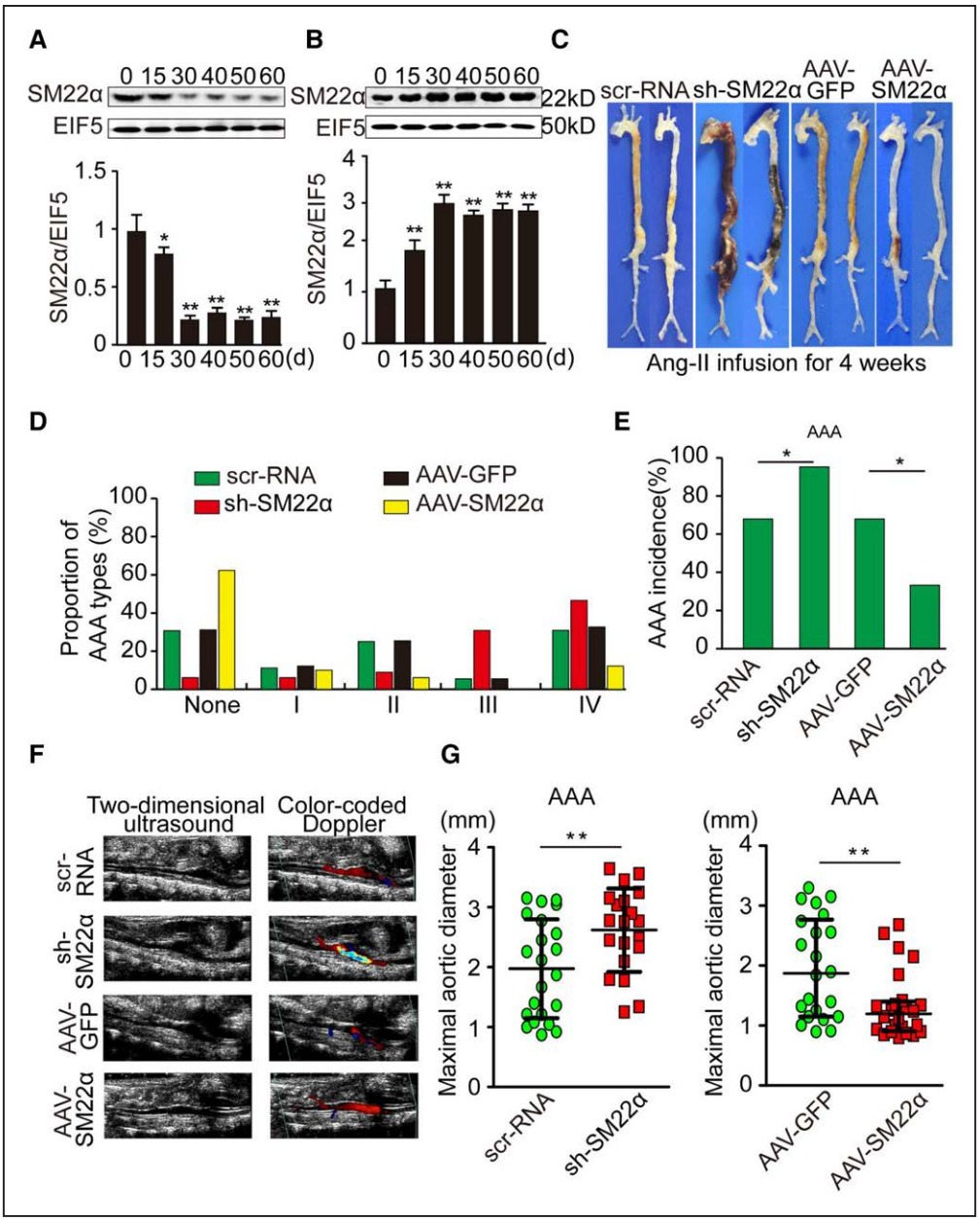

Figure 3. SM22α (smooth muscle 22α) reduction promotes aortic aneurysm (AA) formation, and SM22α overexpression prevents AA formation in Ang II (angiotensin II)-induced AA mice with an ApoE$^{-/-}$ (apolipoprotein E–deficient) background. Male ApoE$^{-/-}$ mice were transfected with Scr-RNA, sh-SM22α, abdominal aortic aneurysm (AAV) GFP (green fluorescent protein), or AAV-SM22α and then treated with Ang II for 28 d (Scr-RNA, n=32; sh-SM22α, n=32; AAV-GFP, n=31; and AAV-SM22α, n=30). **A**, Western blots (WB) for the expression levels of SM22α over time after sh-SM22α transfection in the suprarenal aortas of the Ang II-treated ApoE$^{-/-}$ mice (n=3). **B**, WBs for the expression of SM22α after Ad-GFP-SM22α injection into the suprarenal aortas of the Ang II-treated ApoE$^{-/-}$ mice (n=3). **C**, Representative images of the macroscopic features of AA in the Ang II-treated ApoE$^{-/-}$ mice. **D**, Aneurysm type according to a classification scheme similar to the one described previously.[18] Type IV represents ruptured aneurysms. **E**, Statistical analysis of the abdominal aortic aneurysm (AAA) incidence in the Ang II-treated ApoE$^{-/-}$ mice. **F**, Two-dimensional color-coded ultrasound imaging of aortic aneurysms after 14 d of Ang II treatment. **G**, Maximal AA diameter in the abdominal region in Ang II-treated ApoE$^{-/-}$ mice. Data are presented as the mean±SD. *P<0.05, **P<0.01.

AA classification of I, II, III, and IV, respectively, in the Scr-RNA group; P<0.05; Figure 3C through 3E). AA formation was nearly absent in AAV-SM22α mice compared with that in AAV-GFP mice, which displayed a substantial bulge in the abdominal aorta (10 of 30 mice, 33.3%; 10 AAAs; 3, 3, 0, and 5 with an AA classification of I, II, III, and IV, respectively, in the AAV-SM22α group; 21 of 31 mice, 67.7%; 21 AAAs; 4, 6, 1, and 10 with an AA classification of I, II, III, and IV, respectively, in the AAV-GFP group; P<0.05; Figure 3C through 3E). In addition, the maximal diameters of the descending thoracic aorta (Figure VIA in the online-only Data Supplement) and abdominal aorta (Figure 3G) were substantially higher in the sh-SM22α group than in the Scr-RNA group and were substantially lower in the SM22α overexpression group than in the AAV-GFP group. Correspondingly, the Ang II-induced elastin degradation scores for both the abdominal (Figure 4A and 4B) and descending thoracic (Figure VIB in the online-only

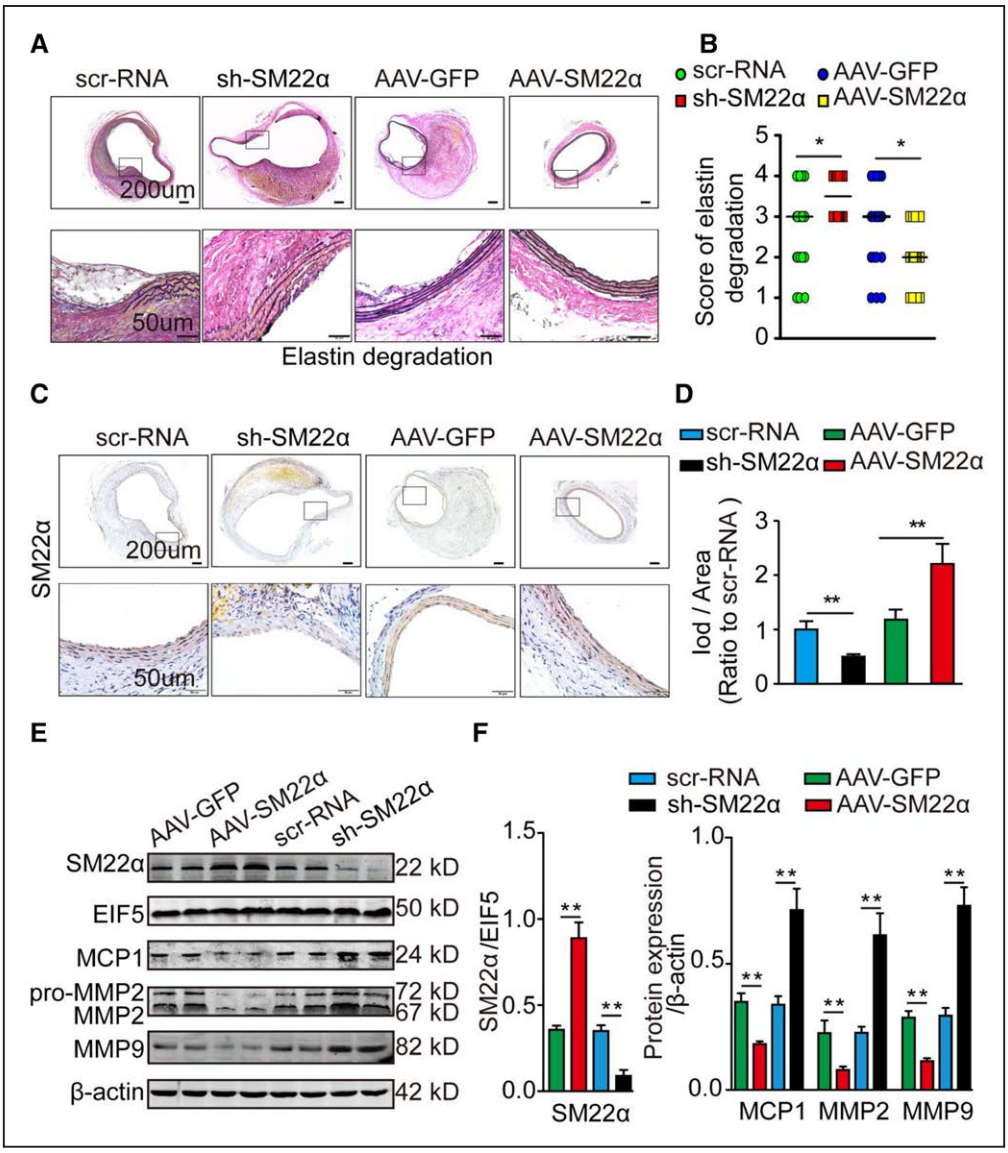

Figure 4. Vascular pathophysiological mechanisms induced by SM22α (smooth muscle 22α) dysregulation in Ang II (angiotensin II)-infusion ApoE$^{-/-}$ (apolipoprotein E–deficient) mice. **A** and **B**, Representative staining with elastin and the elastin degradation score in abdominal aortas of angiotensin-infused male ApoE$^{-/-}$ mice from the 4 groups. Photographs show the location where the most severe elastin degradation occurred (scale bars=200 and 50 μm; magnified photographs). **C** and **D**, Representative staining of the SM22α protein (scale bars=200 and 50 μm) and the corresponding densitometric analysis (n=3). **E** and **F**, Western blots of protein levels and densitometric analysis of aortic SM22α, MCP-1 (monocyte chemotactic protein-1), MMP (matrix metalloproteinase) 2, and MMP9 in the angiotensin-infused male ApoE$^{-/-}$ mice (n=3). Data are presented as the mean±SD. *P<0.05, **P<0.01.

Data Supplement) aortas were significantly higher in the sh-SM22α group than in the Scr-RNA group (P<0.05), with a milder change in the thoracic aorta than in the abdominal aorta. In contrast, elastin degradation in both aortic regions was effectively prevented in AAV-SM22α mice compared with that in AAV-GFP mice. Western blotting results showed that the aortic cleaved caspase-3 expression did not significantly differ between AAV-SM22α and AAV-GFP groups (Figure XIV in the online-only Data Supplement).

On day 28, as anticipated, the aortic SM22α protein levels in all 4 groups were altered (Figure 4E). The aortic protein and mRNA levels of MCP-1, MMP2, and MMP9 and inflammatory cell infiltration were significantly elevated in the sh-SM22α group but were remarkably downregulated in the AAV-SM22α group (P<0.05; Figure 4E and 4F; Figure VIIA through VIIC in the online-only Data Supplement). Similar findings with lower incidence of AAA were obtained in ApoE$^{-/-}$ mice receiving a half dose of Ang II (0.5 μg/kg per minute) infusion for 28 days (Figure VIII in the online-only Data Supplement). Thus, our findings confirmed that the causative role of SM22α deficiency in AA formation occurs partly through enhancing vascular inflammation rather than increasing cell apoptosis. For the murine Ang II-induced AAA model, the first 2 weeks are crucial for aneurysm formation. Therefore, we measured mouse systolic blood pressure levels in a time course. Compared with the sham group, no significant changes on systolic blood pressure were found in sh-SM22α group or AAV-SM22α group (Figure VC and VD in the online-only Data Supplement). To examine the proaneurysmic efficiency of SM22α deficiency

in normolipidemic circumstances, we administered an Ang II infusion to wild-type C57BL/6J mice for 28 days. Consistent with the findings in ApoE$^{-/-}$ mice, after 14 days of Ang II infusion, bulges were detected by 2-dimensional ultrasonography and color-coded Doppler imaging in abdominal aorta from the C57BL/6J mice in sh-SM22α group (Figure 5B). The AAA morbidity (Figure 5A and 5B), maximal aortic diameter (Figure 5C), AAA morbidity (18 of 30 mice; 18 AAAs; 5, 6, 5, and 2 with an AA classification I, II, III, and IV, respectively, in the sh-SM22α group; 5 of 30 mice; 5 AAAs; 1, 1, 0, and 0 with an AA classification of I, II, III, and IV, respectively, in the Scr-RNA group; $P<0.05$; Figure 5D and 5E), SM22α protein expression ($P<0.05$; Figure 5F and 5G), and elastin degradation status ($P<0.05$; Figure 5H) showed similar deteriorated tendencies. Based on these findings, SM22α deficiency was potent enough to instigate AA onset under Ang II therapy in the absence of hyperlipidemia.

Disruption of SM22α Promotes AAA Formation in $CaCl_2$-Infused Mice

To explore whether the effects of vascular SM22α disruption on AAA formation are partially independent of Ang II pathway signaling, we examined the role of SM22α deficiency in the $CaCl_2$-induced AAA model. Three weeks after $CaCl_2$ application in the adventitia of the mouse infrarenal aorta, the maximal aortic diameter (Figure IXA and IXB in the online-only Data Supplement); elastin fragmentation (Figure IXC and IXD in the online-only Data Supplement); the protein expression of SM22α, MCP-1, MMP2, and MMP9; and inflammatory cell infiltration (Figures IXE through IXH and XA through XD in the online-only Data Supplement) detected by Western blotting and immunohistochemical staining showed trends consistent with those found in the aortas of the sh-SM22α group in Ang II-induced AAA. In contrast, overexpression of SM22α remarkably retarded AAA development and the associated inflammatory responses even 6 weeks after $CaCl_2$ stimulation (Figure XI in the online-only Data Supplement). These results indicate that knockdown of SM22α exacerbates AAA formation and related inflammatory pathological changes in a $CaCl_2$-related manner.

SM22α Inhibits ROS Bioactivity and NF-κB Activation

Accumulating lines of evidence have proven that ROS can activate NF-κB, subsequently triggering a cascade of inflammatory responses, including enhanced MMP and MCP-1 expression in various diseases. Thus, we sought to determine whether SM22α disruption promotes proinflammatory molecule expression via the ROS/NF-κB pathway. At 28 days after Ang II infusion, the cytoplasmic levels of p65 and p50 of the NF-κB family were significantly decreased, whereas nuclear p65 and p50 were significantly elevated in the sh-SM22α group than in the Scr-RNA group, indicating a transfer of aortic NF-κB from cytoplasm to nucleus to execute functions as a response to aortic SM22α deficiency. In contrast, the activity of p65 and p50 was suppressed in the AAV-SM22α group (Figure 6C and 6D). Conversely, aortic phosphorylated IκBα (p-IκBα) and IKKβ (p-IKKβ) were reduced on SM22α overexpression and increased on SM22α deficiency (Figure 6A and 6B). Aortic ROS level, as indicated by immunofluorescence staining, exhibited the same significant trends in alterations as those observed for NF-κB expression (Figure 6E and 6F). Nonetheless, there were no obvious changes in the levels of the remaining members of the NF-κB family, including RelB, c-Rel, and p52, in the nucleus and cytoplasm (Figure XII in the online-only Data Supplement).

SM22α Inhibits the Phosphorylation of the p47^{phox} Subunit of Nicotinamide Adenine Dinucleotide Phosphate Oxidase

SM22α disturbance has been demonstrated to facilitate ROS enhancement through promoting p47^{phox} phosphorylation and abnormal cell structure.[26] Based on these findings, we determined whether SM22α deficiency promotes ROS through upregulated p47^{phox} phosphorylation. Immunoprecipitation analysis showed that phosphorylated p47^{phox} was significantly increased as SM22α was deregulated, whereas it was inhibited as SM22α was upregulated (Figure 7A through 7C). Moreover, cytoskeletal structure instability, as reflected by the actin cytoskeletal fraction/cytosolic soluble actin ratio, was significantly decreased in the AAV-SM22α group and significantly increased in the sh-SM22α group compared with that in their respective control groups (Figure 7D). Accordingly, our results demonstrated a causal relationship between SM22α deficiency and 47^{phox} phosphorylation and cytoskeletal destruction, which partially explained the enhanced ROS/NF-κB signaling activation, vascular inflammation, and AAA formation.

Inhibition of NF-κB or ROS Blocks AAA Formation

To determine the obligatory role of the ROS/NF-κB pathway in SM22α deficiency-mediated AAA formation, we performed rescue experiments by separately using NF-κB antagonist SN50 or ROS inhibitor NAC 1 day before 28 days of Ang II infusion in C57BL/6J mice. We observed that compared with PBS administration, either SN50 or NAC administration partially abolished the promoting effect of SM22α deficiency on AAA formation and maximal aortic diameter (Figure 8A through 8G). As anticipated, aortic ROS production was sufficiently inhibited by NAC treatment in SM22α-deficient mice, which was confirmed by a quantitative analysis of the fluorescence signal intensity (Figure 8H and 8I). Western blot analysis revealed that SN50 substantially decreased nuclear p50 and p65, indicating an inhibition of NF-κB (Figure 8J through 8L). Similar trends were observed at 3 weeks after $CaCl_2$ treatment in C57BL/6J mice (Figure XIII in the online-only Data Supplement). Taken together, our results indicated that the ROS/NF-κB pathway is involved in SM22α deficiency-promoted AAA development.

Discussion

In the current study, SM22α overexpression inhibited SMC modulation from a contractile to synthetic phenotype and exerted a protective effect against AAA formation in both Ang II-perfused and $CaCl_2$-induced AAA models. In

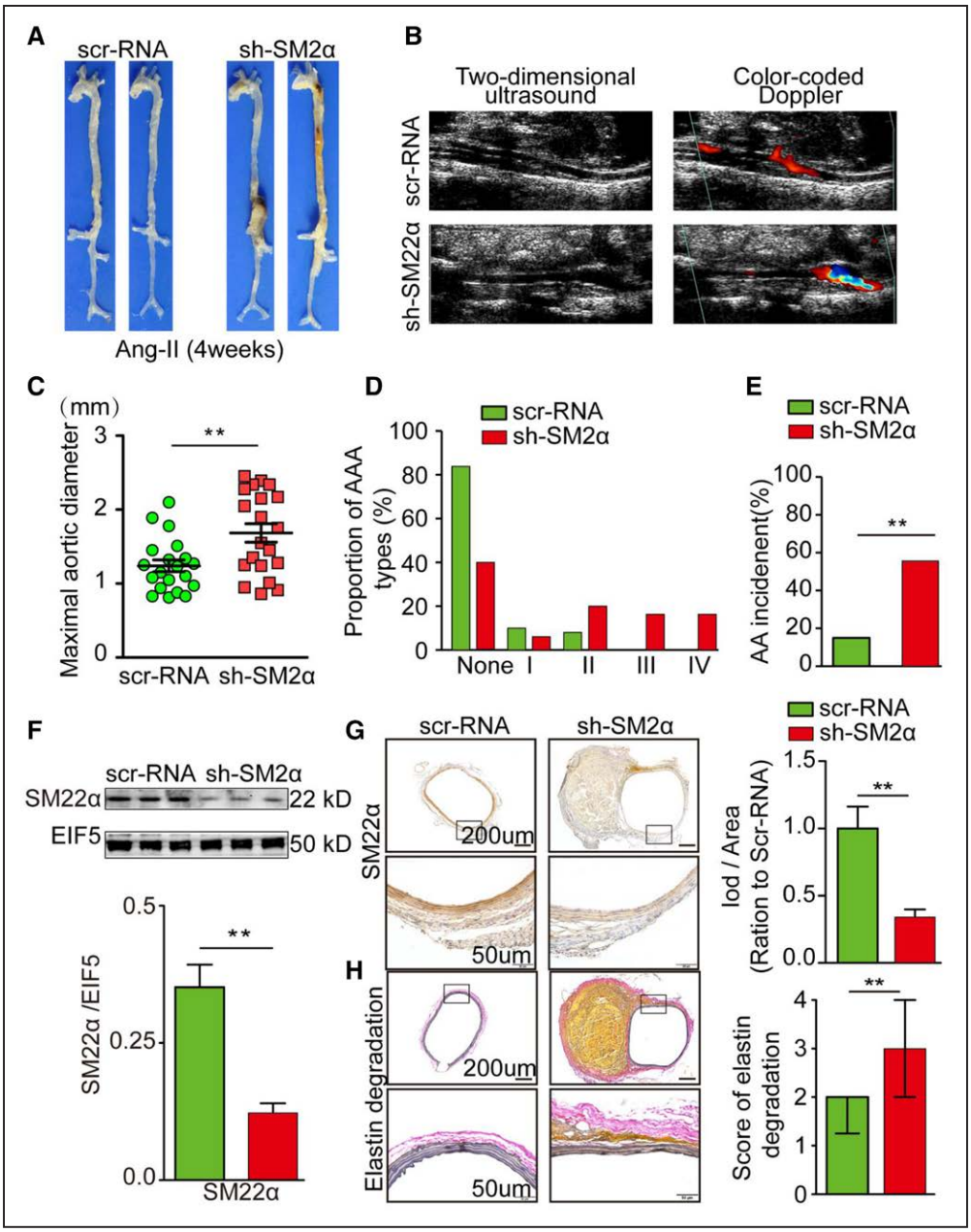

Figure 5. SM22α (smooth muscle 22α) deficiency promotes aortic aneurysm (AA) formation in Ang II (angiotensin II)-infused C57BL/6J mice. Male C57BL/6J mice were treated with Ang II for 28 d, followed by transfection with Scr-RNA or sh-SM22α. Data are presented as the mean±SD, n=30 in each group. **A**, Representative photographs showing AA in Ang II-treated C57BL/6J mice in 2 groups. **B**, Two-dimensional ultrasound and color-coded Doppler imaging of the aortas at the 14th day of Ang II treatment. **C**, Statistical analysis of the AA classification in C57BL/6J mice treated with Ang II. **D**, Aneurysm type according to a classification scheme similar to the one described previously.[18] Type IV represents ruptured aneurysms. **E**, Maximal abdominal aortic aneurysm (AAA) diameter in the Ang II-treated C57BL/6J mice. **F** and **G**, Western blots of the protein levels (**F**), representative staining of the SM22α protein (**G**; scale bars=200 and 50 μm), and the corresponding densitometric analysis in Ang II-treated C57BL/6J mice between 2 groups (n=3). **H**, Representative staining with elastin and the elastin degradation score in aortas from C57BL/6J mice treated with Ang II (scale bars=200 and 50 μm). The presented photographs were obtained at the location where the most severe elastin degradation occurred. Data are presented as the mean±SD. ***P*<0.01.

contrast, SM22α knockdown exacerbated this SMC switching and AAA formation. Consistent trends were also found in extended models using half-dose Ang II-infused mice and $CaCl_2$-treated mice after 6 weeks. The mechanisms underlying this phenomenon were demonstrated in the findings that DNA hypermethylation-associated SM22α deficiency could activate the aortic ROS/NF-κB pathway and proinflammatory and matrix proteolytic molecules MCP-1 and MMPs. These changes provided a vascular environment susceptible to inflammation and predisposed the aorta to aneurismal formation.

With the increased awareness of disease prevention and advanced technology for the detection and diagnosis of AAA, the incidence of small, insidious AAA (≤5 cm in diameter) has markedly increased.[27] Despite the consensus that the best strategy for AAA management emphasizes early intervention,[28] limited progress has been made in managing patients with small AAA because there are no effective drugs for preventing and

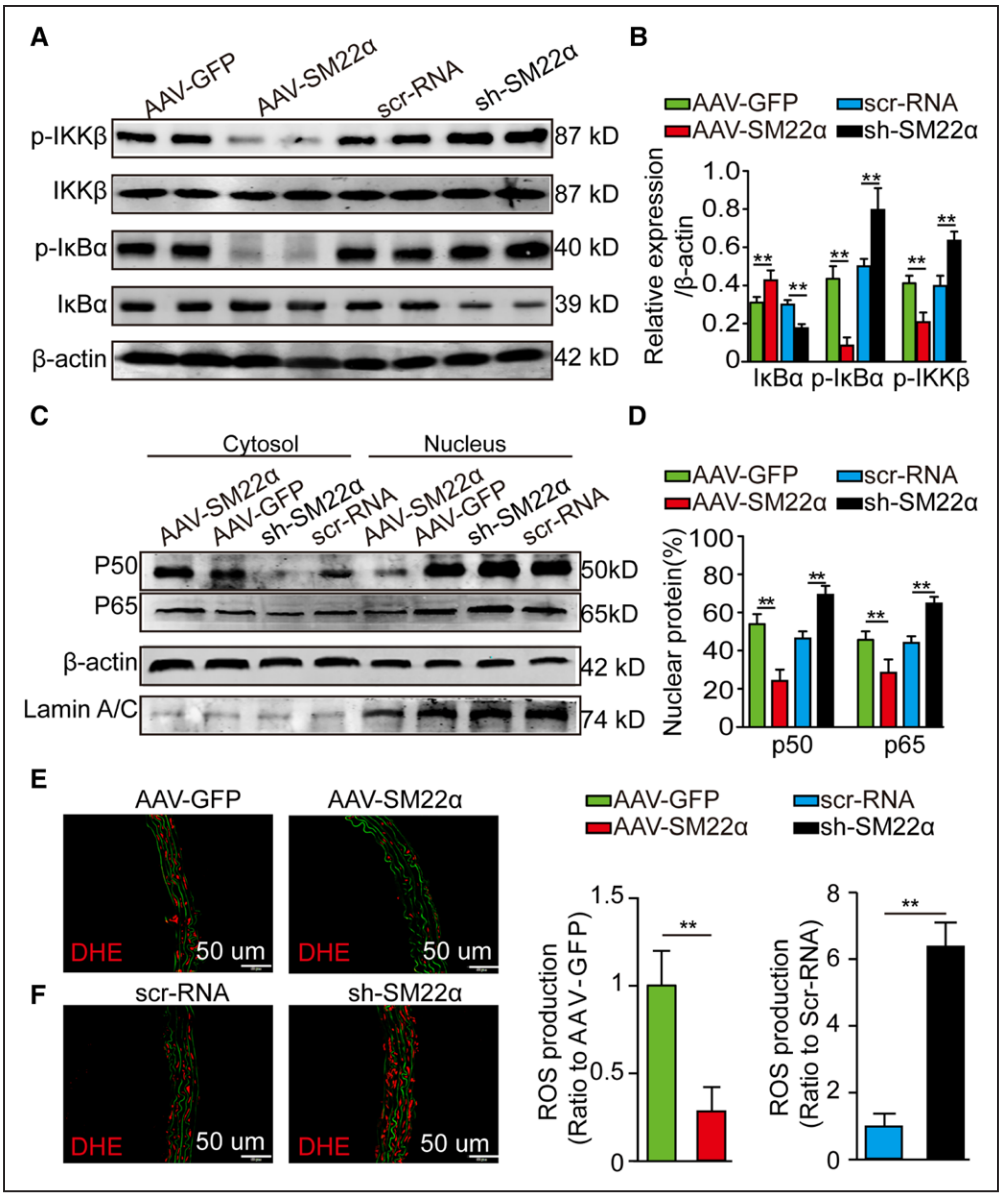

Figure 6. Reduction of SM22α (smooth muscle 22α) enhances reactive oxygen species (ROS) bioactivity and activates NF-κB (nuclear factor-κB) in Ang II (angiotensin II)-infused ApoE$^{-/-}$ (apolipoprotein E–deficient) mice. Male ApoE$^{-/-}$ mice were treated with Ang II for 28 d, followed by different SM22α modulations. **A** and **B**, Representative Western blots of the total and phosphorylated content of IκBα (nuclear factor of κ light polypeptide gene enhancer in B-cells inhibitor-α) and IKKβ (inhibitor of NF-κB kinase subunit-β; n=5), and statistical analysis (**B**) on SM22α modulation. **C** and **D**, Cytoplasmic and nuclear expression of p50 and p65 (n=5; **C**) and statistical analysis (**D**) in aortas from the 4 groups of mice. **E** and **F**, In situ dihydroethidium (DHE) staining of the aortas from ApoE$^{-/-}$ mice after 28 d of Ang II perfusion (elastin fiber, green; ROS, red). All sections are shown with the lumen above (scale bars=50 μm). **F**, Statistical analysis of ROS production in the aortas from Ang II-induced ApoE$^{-/-}$ mice on SM22α modulation (n=5; scale bars=100 and 50 μm). Data are presented as the mean±SD. $^{**}P<0.01$.

reversing AAA advancement.[29,30] Vascular pathology mediated by SMC phenotypic switching plays a vital role during AAA formation.[8,31,32] In previous studies, SM22α has generally been considered one of the hallmarks of SMC phenotypic switching.[8,33] However, whether SM22α has interventional value in AAA management remains unexplored. In our study, SM22α protected against AAA initiation through inhibiting the activation of the ROS pathway in 2 well-accepted AAA models, whereas SM22α knockdown intensified AAA formation. Our study confirms a crucial role of SM22α in AAA development other than its role as a biomarker of SMC structure. Our study, combined with others elucidating the role of SM22α in vessels, highlights the significance of SM22α in maintaining vascular integrity and function,[34–37] thus indicating the great therapeutic potential of targeting SM22α in the treatment of vascular diseases. Moreover, this finding provides a new direction for effective/potential treatments for AAA. Theoretically, detection of and preventative interventions against pathogenic factors during the inchoate stage of a disease are more advantageous for intercepting further pathogenic deterioration and thus protecting against later manifestations and progression when the disease has already formed. SMC apoptosis certainly represents a critical pathophysiological process[9,38]; however, it occurs in a relatively late phase during AAA development.[39]

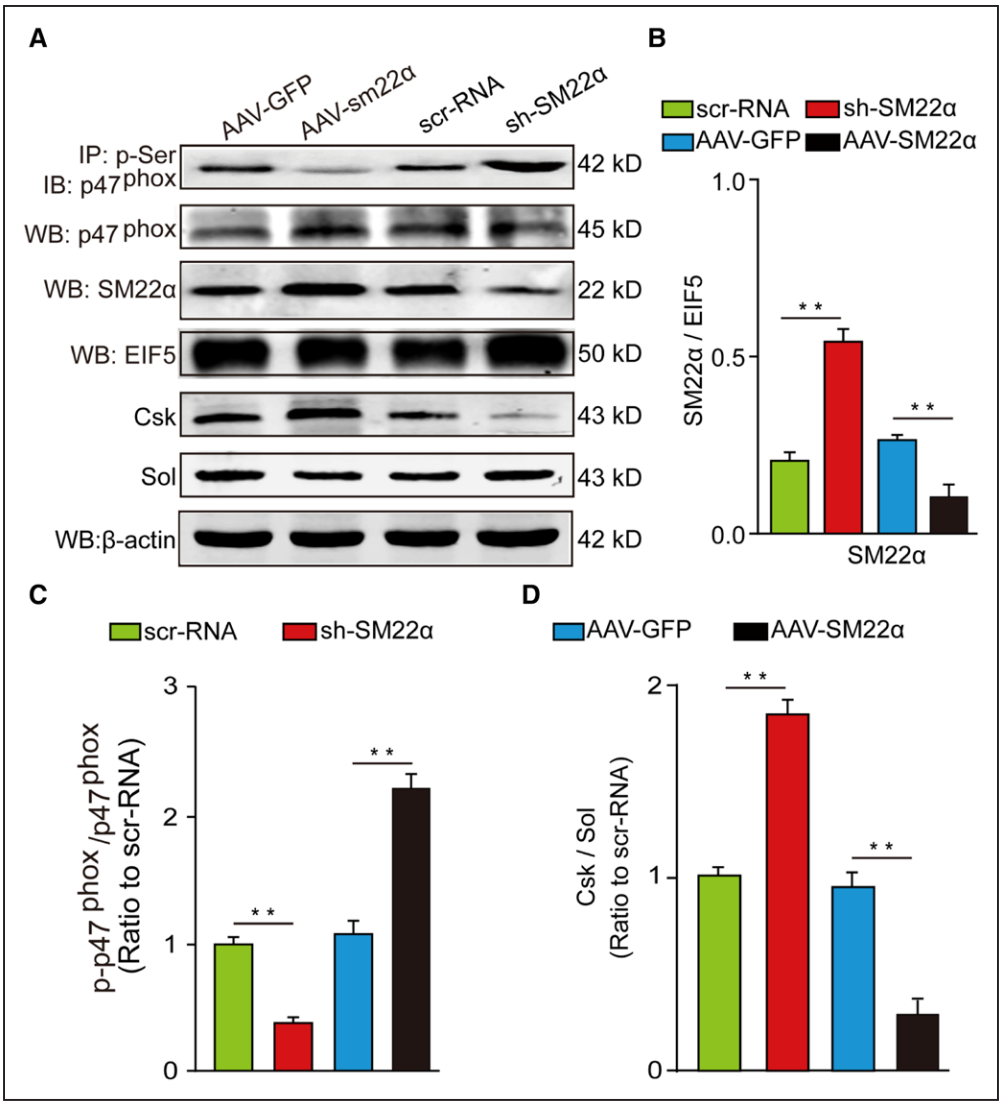

Figure 7. SM22α (smooth muscle 22α) deficiency promotes phosphorylation of the p47^{phox} subunit of nicotinamide adenine dinucleotide phosphate oxidase and destroys the cytoskeletal structure. **A**, Representative Western blots (WB) results of the aortas of Ang II (angiotensin II)-induced male ApoE$^{-/-}$ (apolipoprotein E–deficient) mice. **B**, Densitometric analysis of aortic SM22α protein expression. **C**, Statistical analysis of the WB results of the phosphorylated p47^{phox} to total p47^{phox} ratio (p-p47^{phox}/p47^{phox}) in mice aortas. **D**, Statistical analysis of the WB results of the vascular smooth muscle cell cytoskeletal actin to cytosolic soluble actin (Csk/Sol) ratio (n=3). Data are presented as the mean±SD. $^{**}P<0.01$. EIF5 indicates eukaryotic translation initiation factor 5; IB, immunoblotting; and IP, immunoprecipitation.

In agreement with former studies, we also found that SM22α expression was reduced in the early days in both models. This observation, along with those of earlier works, indicates that SMC phenotypic switching might be an early triggering event in AAA pathogenesis.[9] In addition, this kind of SMC transition was associated with significantly higher DNA hypermethylation in the *SM22α* promoter region, which was detected as early as the fifth day of Ang II intervention and remained stable until the seventh day. Given that epigenetic alterations in gene promoters (such as DNA hypermethylation) occur even ahead of aberrant gene expression and that DNA hypermethylation is regarded as a stable DNA modification,[40,41] *SM22α* promoter hypermethylation might be a potential robust marker for the recognition of early AAA formation or progression risk.

Mechanistically, we found aberrant NF-κB activation, an abnormal inflammatory response, and MMP fluctuation under SM22α dysregulation in both AAA models. Our study reveals the ability of SM22α to influence the above inflammatory molecules and MMPs in AAA models. In agreement with our findings, SM22α deficiency was previously shown to contribute to increased macrophage infiltration in an atherosclerosis model and to promote proinflammatory genes and MMP2/9 expression in mouse carotid intimal injuries.[37,42,43] These results might provide theoretical clues on how adventitial inflammatory cell accumulation develops into transmural vascular inflammation. Medial SMC phenotypic switching might even advance with the help of early inflammatory activation from the aortic adventitia because SMCs can undergo phenotypic switching in response to multiple inflammatory cytokines.[44] In turn, this SMC switching might further mediate medial aortic inflammatory cell infiltration and MMP secretion, thus facilitating AAA development.

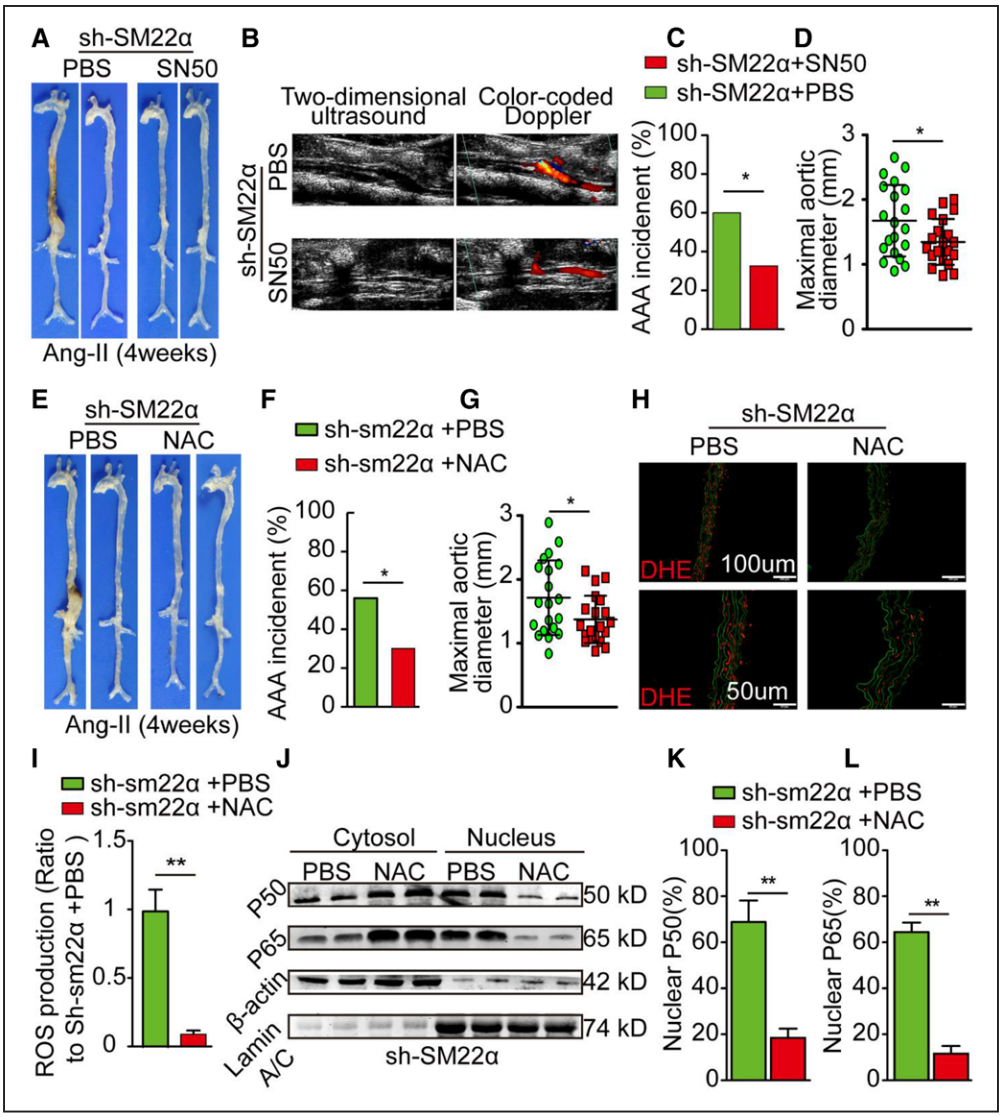

Figure 8. Suppression of reactive oxygen species (ROS) or NF-κB (nuclear factor-κB) alleviates the promotional effect of SM22α (smooth muscle 22α) deficiency on Ang II (angiotensin II)-induced abdominal aortic aneurysm (AAA) formation. **A**–**D**, Male C57BL/6J mice transfected with sh-SM22α were treated with the NF-κB inhibitor SN50 or PBS, and then mice were infused with Ang II for 28 d (n=30 in each group). **A**, Representative photographs showing the macroscopic features of aortic aneurysms in male Ang II-induced C57BL/6J mice. **B**, Ultrasound and Doppler imaging of aortic aneurysms after 14 d of Ang II treatment. **C**, AAA incidence. **D**, Maximal aortic diameter of the 2 groups of Ang II-induced C57BL/6J mice. **E**–**L**, Male C57BL/6J mice transfected with sh-SM22α were treated with either the ROS antagonist N-acetylcysteine (NAC) or PBS, and then they were infused with Ang II for 28 d (n=30 in each group). **E**, Representative photographs showing the macroscopic features of aortic aneurysms. **F** and **G**, Statistical analysis of mouse aortic aneurysm morbidity (**F**) and the maximal aortic diameter (**G**) in Ang II-infused C57BL/6J mice. **H** and **I**, In situ dihydroethidium (DHE) staining of mouse aortas (elastin fiber, green; ROS, red). All sections are shown with the lumen above (scale bars=100 and 50 μm; **H**) and the corresponding statistical analysis of ROS production (**I**) in aortas on sh-SM22α or Scr-RNA transfection (n=5; scale bars=100 and 50 μm). **J**–**L**, Representative Western blots of the cytoplasmic and nuclear expression of p50 and p65 (n=3; **J**) and the statistical analysis of nuclear p50 (**K**) and p65 (**L**) in Ang II-treated mice after SM22α modulation and NAC treatment. Data are presented as the mean±SD. *P<0.05, **P<0.01.

We further explored the upstream molecule essential for NF-κB activation. In our study, SM22α knockdown stimulated actin cytoskeleton disorganization, increasing phosphorylated p47^{phox}—the centrally functioning subunit of nicotinamide adenine dinucleotide phosphate oxidase—and triggering the cascade of ROS production.[26,37] We revealed a role for SM22α insufficiency in promoting ROS generation and subsequent NF-κB activation in AAA. Consistently, a number of studies have confirmed the role of this signaling pathway in SM22α-knockdown mice. Using a carotid injury model, Shen et al[37] found that the systemic knockout of SM22α increases the cellular ROS level possibly through disordered actin arrangement, consequently activating NF-κB and its downstream proinflammatory genes. Additionally, another study found that the knockdown of SM22α triggers actin cytoskeleton disorganization in VSMCs, increasing the phosphorylation of p47^{phox}—a central subunit of nicotinamide adenine dinucleotide phosphate oxidase—and enhancing intracellular ROS levels.[26] Our observations indicate that cytoskeletal remodeling induced by SM22α disruption may activate ROS production and enhance downstream NF-κB in the context of AAA.

Next, we verified whether this ROS/NF-κB pathway is indispensable in associating SM22α knockdown with AAA

formation by using the antagonist SN50 or inhibitor NAC. We found that SN50 or NAC partially reversed the SM22α deficiency-exacerbated AAA formation, as well as the related vascular pathophysiological changes, namely, elevated aortic MMP2/9 and proinflammatory molecule levels. Previous studies showed that SM22α loss of function resulted in enhanced expression of proinflammatory genes that are governed by NF-κB in aortic VSMCs.[26,37] Our results, along with multiple previous studies reporting that SM22α knockdown could activate the ROS/NF-κB pathway,[26] confirm the crucial role of the NF-κB pathway in strengthening the abovementioned proinflammatory factors and MMP2/9 elevation in SM22α deficiency-mediated SMC phenotypic switching in AAA formation. Nonetheless, other mechanisms await investigation. A recent report suggested that SM22α promotes the phosphorylation and activation of SIRT1 (sirtuin 1) by recruiting CKII (casein kinase II) and SIRT1, which augments the anti-inflammatory effect of SIRT1 and is considered effective for suppressing AAA development.[43] Our study along with earlier works thoroughly demonstrates the role of disturbed SM22α in vascular disorder development and indicates that SM22α has great potential for therapeutic intervention.

This study has some limitations. First, the exact mechanisms remain unsolved and require additional research for further illumination. Second, in our experiment, SM22α was systemically affected, not specific to VSMCs. Although SM22α overexpression in adventitial fibroblasts may induce their transition to myofibroblasts that secrete various cytokines and inflammatory molecules, previous studies have suggested that this transition is mainly instigated by vascular ROS activation.[25] Because excessive SM22α in VSMCs was demonstrated to reduce vascular ROS level,[37,43,45] this transition might be hindered and even abrogated by the low level of ROS as a result of VSMC SM22α overexpression.

In conclusion, we confirm that SM22α downregulation has a causative role in AAA formation, which is mediated through internally instigated SMC phenotypic switching by activation of the ROS/NF-κB pathway. In addition, DNA hypermethylation is associated with AAA formation by affecting the SM22α expression level. These inchoate changes might be biochemically detectable before the catastrophic disturbance leading to AAA, contributing a novel and promising target for early AAA detection and intervention.

Acknowledgments

We thank Yili Sun and Xiangshi Li for their technical help.

Sources of Funding

This work was supported by grants to J. Bin from the National Natural Science Foundation of China (No. 81771857, No. 81571698, and No. 81271640).

Disclosures

None.

References

1. Thom T, Haase N, Rosamond W, et al; American Heart Association Statistics Committee and Stroke Statistics Subcommittee. Heart disease and stroke statistics–2006 update: a report from the American Heart Association Statistics Committee and Stroke Statistics Subcommittee. *Circulation*. 2006;113:e85–e151. doi: 10.1161/CIRCULATIONAHA.105.171600
2. Golledge J, Norman PE. Current status of medical management for abdominal aortic aneurysm. *Atherosclerosis*. 2011;217:57–63. doi: 10.1016/j.atherosclerosis.2011.03.006
3. Krueger F, Kappert K, Foryst-Ludwig A, Kramer F, Clemenz M, Grzesiak A, Sommerfeld M, Paul Frese J, Greiner A, Kintscher U, Unger T, Kaschina E. AT1-receptor blockade attenuates outward aortic remodeling associated with diet-induced obesity in mice. *Clin Sci (Lond)*. 2017;131:1989–2005. doi: 10.1042/CS20170131
4. Daugherty A, Manning MW, Cassis LA. Angiotensin II promotes atherosclerotic lesions and aneurysms in apolipoprotein E-deficient mice. *J Clin Invest*. 2000;105:1605–1612. doi: 10.1172/JCI7818
5. Davis FM, Rateri DL, Daugherty A. Mechanisms of aortic aneurysm formation: translating preclinical studies into clinical therapies. *Heart*. 2014;100:1498–1505. doi: 10.1136/heartjnl-2014-305648
6. Malekzadeh S, Fraga-Silva RA, Trachet B, Montecucco F, Mach F, Stergiopulos N. Role of the renin-angiotensin system on abdominal aortic aneurysms. *Eur J Clin Invest*. 2013;43:1328–1338. doi: 10.1111/eci.12173
7. Ferguson CD, Clancy P, Bourke B, Walker PJ, Dear A, Buckenham T, Norman P, Golledge J. Association of statin prescription with small abdominal aortic aneurysm progression. *Am Heart J*. 2010;159:307–313. doi: 10.1016/j.ahj.2009.11.016
8. Salmon M, Johnston WF, Woo A, Pope NH, Su G, Upchurch GR Jr, Owens GK, Ailawadi G. KLF4 regulates abdominal aortic aneurysm morphology and deletion attenuates aneurysm formation. *Circulation*. 2013;128(11 suppl 1):S163–S174. doi: 10.1161/CIRCULATIONAHA.112.000238
9. Ailawadi G, Moehle CW, Pei H, Walton SP, Yang Z, Kron IL, Lau CL, Owens GK. Smooth muscle phenotypic modulation is an early event in aortic aneurysms. *J Thorac Cardiovasc Surg*. 2009;138:1392–1399. doi: 10.1016/j.jtcvs.2009.07.075
10. Lenk GM, Tromp G, Weinsheimer S, Gatalica Z, Berguer R, Kuivaniemi H. Whole genome expression profiling reveals a significant role for immune function in human abdominal aortic aneurysms. *BMC Genomics*. 2007;8:237. doi: 10.1186/1471-2164-8-237
11. Yoshimura K, Aoki H, Ikeda Y, Fujii K, Akiyama N, Furutani A, Hoshii Y, Tanaka N, Ricci R, Ishihara T, Esato K, Hamano K, Matsuzaki M. Regression of abdominal aortic aneurysm by inhibition of c-Jun N-terminal kinase. *Nat Med*. 2005;11:1330–1338. doi: 10.1038/nm1335
12. Yamashita O, Yoshimura K, Nagasawa A, Ueda K, Morikage N, Ikeda Y, Hamano K. Periostin links mechanical strain to inflammation in abdominal aortic aneurysm. *PLoS One*. 2013;8:e79753. doi: 10.1371/journal.pone.0079753
13. Robinet P, Milewicz DM, Cassis LA, Leeper NJ, Lu HS, Smith JD. Consideration of sex differences in design and reporting of experimental arterial pathology studies-statement From ATVB council. *Arterioscler Thromb Vasc Biol*. 2018;38:292–303. doi: 10.1161/ATVBAHA.117.309524
14. Trivedi DB, Loftin CD, Clark J, Myers P, DeGraff LM, Cheng J, Zeldin DC, Langenbach R. β-Arrestin-2 deficiency attenuates abdominal aortic aneurysm formation in mice. *Circ Res*. 2013;112:1219–1229. doi: 10.1161/CIRCRESAHA.112.280399
15. Longo GM, Xiong W, Greiner TC, Zhao Y, Fiotti N, Baxter BT. Matrix metalloproteinases 2 and 9 work in concert to produce aortic aneurysms. *J Clin Invest*. 2002;110:625–632. doi: 10.1172/JCI15334
16. O'Sullivan AW, Wang JH, Redmond HP. NF-kappaB and p38 MAPK inhibition improve survival in endotoxin shock and in a cecal ligation and puncture model of sepsis in combination with antibiotic therapy. *J Surg Res*. 2009;152:46–53. doi: 10.1016/j.jss.2008.04.030
17. Vieira GLT, Lossie AC, Lay DC Jr, Radcliffe JS, Garner JP. Preventing, treating, and predicting barbering: a fundamental role for biomarkers of oxidative stress in a mouse model of Trichotillomania. *PLoS One*. 2017;12:e0175222. doi: 10.1371/journal.pone.0175222
18. Daugherty A, Manning MW, Cassis LA. Antagonism of AT2 receptors augments angiotensin II-induced abdominal aortic aneurysms and atherosclerosis. *Br J Pharmacol*. 2001;134:865–870. doi: 10.1038/sj.bjp.0704331
19. Wang Y, Ait-Oufella H, Herbin O, Bonnin P, Ramkhelawon B, Taleb S, Huang J, Offenstadt G, Combadière C, Rénia L, Johnson JL, Tharaux PL, Tedgui A, Mallat Z. TGF-beta activity protects against inflammatory aortic aneurysm progression and complications in angiotensin II-infused mice. *J Clin Invest*. 2010;120:422–432. doi: 10.1172/JCI38136
20. Su SJ, Huang LW, Pai LS, Liu HW, Chang KL. Homocysteine at pathophysiologic concentrations activates human monocyte and induces cytokine expression and inhibits macrophage migration inhibitory factor expression. *Nutrition*. 2005;21:994–1002. doi: 10.1016/j.nut.2005.01.011

21. Krishna SM, Seto SW, Jose RJ, Li J, Morton SK, Biros E, Wang Y, Nsengiyumva V, Lindeman JH, Loots GG, Rush CM, Craig JM, Golledge J. Wnt signaling pathway inhibitor sclerostin inhibits angiotensin II-induced aortic aneurysm and atherosclerosis. *Arterioscler Thromb Vasc Biol*. 2017;37:553–566. doi: 10.1161/ATVBAHA.116.308723
22. Guo S, Shen S, Wang J, Wang H, Li M, Liu Y, Hou F, Liao Y, Bin J. Detection of high-risk atherosclerotic plaques with ultrasound molecular imaging of glycoprotein IIb/IIIa receptor on activated platelets. *Theranostics*. 2015;5:418–430. doi: 10.7150/thno.10020
23. Satoh K, Nigro P, Matoba T, O'Dell MR, Cui Z, Shi X, Mohan A, Yan C, Abe J, Illig KA, Berk BC. Cyclophilin A enhances vascular oxidative stress and the development of angiotensin II-induced aortic aneurysms. *Nat Med*. 2009;15:649–656. doi: 10.1038/nm.1958
24. Chen Y, Zhang C, Shen S, Guo S, Zhong L, Li X, Chen G, Chen G, He X, Huang C, He N, Liao W, Liao Y, Bin J. Ultrasound-targeted microbubble destruction enhances delayed BMC delivery and attenuates post-infarction cardiac remodelling by inducing engraftment signals. *Clin Sci (Lond)*. 2016;130:2105–2120. doi: 10.1042/CS20160085
25. Liu Z, Luo H, Zhang L, Huang Y, Liu B, Ma K, Feng J, Xie J, Zheng J, Hu J, Zhan S, Zhu Y, Xu Q, Kong W, Wang X. Hyperhomocysteinemia exaggerates adventitial inflammation and angiotensin II-induced abdominal aortic aneurysm in mice. *Circ Res*. 2012;111:1261–1273. doi: 10.1161/CIRCRESAHA.112.270520
26. Lv P, Miao SB, Shu YN, Dong LH, Liu G, Xie XL, Gao M, Wang YC, Yin YJ, Wang XJ, Han M. Phosphorylation of smooth muscle 22α facilitates angiotensin II-induced ROS production via activation of the PKCδ-P47phox axis through release of PKCδ and actin dynamics and is associated with hypertrophy and hyperplasia of vascular smooth muscle cells in vitro and in vivo. *Circ Res*. 2012;111:697–707. doi: 10.1161/CIRCRESAHA.112.272013
27. Baxter BT, Terrin MC, Dalman RL. Medical management of small abdominal aortic aneurysms. *Circulation*. 2008;117:1883–1889. doi: 10.1161/CIRCULATIONAHA.107.735274
28. Golledge J, Muller J, Daugherty A, Norman P. Abdominal aortic aneurysm: pathogenesis and implications for management. *Arterioscler Thromb Vasc Biol*. 2006;26:2605–2613. doi: 10.1161/01.ATV.0000245819.32762.cb
29. Powell JT, Brady AR. Detection, management, and prospects for the medical treatment of small abdominal aortic aneurysms. *Arterioscler Thromb Vasc Biol*. 2004;24:241–245. doi: 10.1161/01.ATV.0000106016.13624.4a
30. Golledge J, Muller J, Shephard N, Clancy P, Smallwood L, Moran C, Dear AE, Palmer LJ, Norman PE. Association between osteopontin and human abdominal aortic aneurysm. *Arterioscler Thromb Vasc Biol*. 2007;27:655–660. doi: 10.1161/01.ATV.0000255560.49503.4e
31. Guo DC, Pannu H, Tran-Fadulu V, et al. Mutations in smooth muscle alpha-actin (ACTA2) lead to thoracic aortic aneurysms and dissections. *Nat Genet*. 2007;39:1488–1493. doi: 10.1038/ng.2007.6
32. Liu R, Lo L, Lay AJ, et al. ARHGAP18 protects against thoracic aortic aneurysm formation by mitigating the synthetic and proinflammatory smooth muscle cell phenotype. *Circ Res*. 2017;121:512–524. doi: 10.1161/CIRCRESAHA.117.310692
33. Li L, Miano JM, Cserjesi P, Olson EN. SM22 alpha, a marker of adult smooth muscle, is expressed in multiple myogenic lineages during embryogenesis. *Circ Res*. 1996;78:188–195.
34. Shanahan CM, Cary NR, Metcalfe JC, Weissberg PL. High expression of genes for calcification-regulating proteins in human atherosclerotic plaques. *J Clin Invest*. 1994;93:2393–2402. doi: 10.1172/JCI117246
35. Wamhoff BR, Hoofnagle MH, Burns A, Sinha S, McDonald OG, Owens GK. A G/C element mediates repression of the SM22alpha promoter within phenotypically modulated smooth muscle cells in experimental atherosclerosis. *Circ Res*. 2004;95:981–988. doi: 10.1161/01.RES.0000147961.09840.fb
36. Feil S, Hofmann F, Feil R. SM22alpha modulates vascular smooth muscle cell phenotype during atherogenesis. *Circ Res*. 2004;94:863–865. doi: 10.1161/01.RES.0000126417.38728.F6
37. Shen J, Yang M, Ju D, Jiang H, Zheng JP, Xu Z, Li L. Disruption of SM22 promotes inflammation after artery injury via nuclear factor kappaB activation. *Circ Res*. 2010;106:1351–1362. doi: 10.1161/CIRCRESAHA.109.213900
38. Kunieda T, Minamino T, Nishi J, Tateno K, Oyama T, Katsuno T, Miyauchi H, Orimo M, Okada S, Takamura M, Nagai T, Kaneko S, Komuro I. Angiotensin II induces premature senescence of vascular smooth muscle cells and accelerates the development of atherosclerosis via a p21-dependent pathway. *Circulation*. 2006;114:953–960. doi: 10.1161/CIRCULATIONAHA.106.626606
39. Daugherty A, Cassis LA, Lu H. Complex pathologies of angiotensin II-induced abdominal aortic aneurysms. *J Zhejiang Univ Sci B*. 2011;12:624–628. doi: 10.1631/jzus.B1101002
40. Cedar H, Bergman Y. Linking DNA methylation and histone modification: patterns and paradigms. *Nat Rev Genet*. 2009;10:295–304. doi: 10.1038/nrg2540
41. Esteller M. Cancer epigenomics: DNA methylomes and histone-modification maps. *Nat Rev Genet*. 2007;8:286–298. doi: 10.1038/nrg2005
42. Chen R, Zhang F, Song L, Shu Y, Lin Y, Dong L, Nie X, Zhang D, Chen P, Han M. Transcriptome profiling reveals that the SM22α-regulated molecular pathways contribute to vascular pathology. *J Mol Cell Cardiol*. 2014;72:263–272. doi: 10.1016/j.yjmcc.2014.04.003
43. Shu YN, Dong LH, Li H, et al. CKII-SIRT1-SM22α loop evokes a self-limited inflammatory response in vascular smooth muscle cells. *Cardiovasc Res*. 2017;113:1198–1207. doi: 10.1093/cvr/cvx048
44. Salmon M, Gomez D, Greene E, Shankman L, Owens GK. Cooperative binding of KLF4, pELK-1, and HDAC2 to a G/C repressor element in the SM22α promoter mediates transcriptional silencing during SMC phenotypic switching in vivo. *Circ Res*. 2012;111:685–696. doi: 10.1161/CIRCRESAHA.112.269811
45. Shu YN, Zhang F, Bi W, Dong LH, Zhang DD, Chen R, Lv P, Xie XL, Lin YL, Xue ZY, Li H, Miao SB, Zhao LL, Wang H, Han M. SM22α inhibits vascular inflammation via stabilization of IκBα in vascular smooth muscle cells. *J Mol Cell Cardiol*. 2015;84:191–199. doi: 10.1016/j.yjmcc.2015.04.020

Highlights

- Decreased SM22α (smooth muscle 22α) expression in abdominal aortic aneurysm tissues is closely associated with the hypermethylation state of its gene promoter.
- SM22α protects against abdominal aortic aneurysm formation by attenuating vascular inflammation in 2 kinds of abdominal aortic aneurysm model.
- The anti-inflammation property of SM22α may be mediated through decreasing the phosphorylation of the $p47^{phox}$ subunit in nicotinamide adenine dinucleotide phosphate oxidase, which downregulates reactive oxygen species production and further prevents NF-κB (nuclear factor-κB) activation.